Peer reviewed version

Link to published version (if available):

Link to publication record in Explore Bristol Research
PDF-document

University of Bristol - Explore Bristol Research
General rights

Comparison of OTFS and OFDM in Ray Launched sub-6 GHz and mmWave Line-of-Sight Mobility Channels

Fred Wiffen*, Lawrence Sayer*, Mohammud Z. Bocus†, Angela Doufexi*, Andrew Nix*

*Communication Systems & Networks Research Group, University of Bristol, Bristol, UK

†Toshiba Research Europe Limited, Bristol, UK

Abstract—Orthogonal Time Frequency Space (OTFS) is a recently proposed modulation scheme for doubly-dispersive channels in which symbol multiplexing and processing is performed in the Doppler-delay domain, rather than conventional time-frequency domain. In this paper, the performance of OTFS is compared to orthogonal frequency division multiplexing (OFDM) for line-of-sight mobility automotive channels. Ray launching is used to simulate the channel for two different dynamic 3D vehicle to infrastructure transmission environments, using a Kirchhoff model for diffuse scattering from rough surfaces. Bit level simulations for transmission from a transmitter moving at speeds of 13 m/s and 31 m/s are then carried out, for both OFDM and OTFS. We find that with short length block codes OTFS outperforms OFDM in all simulated scenarios, reducing the block error rate by more than 50% on average. Unlike previous work, simulations are performed in the time domain using practical rectangular pulse shapes, rather than theoretical 'ideal pulses'. We provide an analysis of these pulses, and derive relevant expressions for the doubly dispersive channel in terms of the multipath delays and Doppler shifts.

I. Introduction

With 5G communication services aiming to provide ubiquitous network access, there is a growing need for communication systems capable of providing good quality of service wireless access in high mobility environments, i.e., to and from moving vehicles. These mobile environments are characterised by having a wireless channel that is doubly dispersive - spreading signals across both time, due to the delay of the propagation paths, and frequency, due to Doppler shifts caused by motion in the channel. This is problematic for conventional waveforms such as OFDM, which suffer from heavy fading in a rapidly varying channel.

Recently, the Orthogonal Time Frequency Space (OTFS) modulation scheme was proposed as a solution to these issues [1]. The main innovation of the OTFS waveform is that, unlike conventional waveforms, which operate in the time-frequency domain, in OTFS symbol multiplexing and detection is performed across a grid in the 'Doppler-delay' domain. Viewed in this domain, the channel response is decomposed into a slowly varying response that closely reflects the physical geometry of the channel. A Doppler-delay impulse transmitted through the channel appears after demodulation as a series of impulses translated according to the delays and Doppler shifts of the constituent propagation paths. Providing the resolution is sufficient to separate the received signal components, fading is eliminated and the full diversity of the channel is captured with each transmitted symbol experiencing the same channel gain (assuming ideal pulse-shaping). In addition, OTFS can be implemented as a pre- and post-processing stage to standard multicarrier modulation schemes, enabling it to co-exist with other 5G technologies.

In this work, we provide a performance comparison of OTFS and standard OFDM at both sub-6 GHz and mmWave using ray launched line-of-sight channels captured for two automotive mobility scenarios namely a built up urban environment and a motorway environment.

II. Related Work

In [1], system level simulations of OFDM and OTFS were performed using a 3GPP rural macrocell channel model, for transmission to vehicles moving at speeds of 30, 120 and 500 km/h. Using a configuration compliant with 4G LTE specifications, the authors show a 2-3 dB improvement in coded block error rate, increasing up to around 5 dB when shorter coding blocks were used. The effect of inter-carrier interference, with and without compensation, on both waveforms was also studied. However, little detail is given on the algorithms used for equalisation or the exact pulse shaping method used. In [2] the authors extend the study to millimetre wave transmission, and show that OTFS again outperforms OFDM by around 5 dB, with OTFS performance improving as the subcarrier spacing is increased.

In [3] a low complexity message passing based equaliser is applied in the Doppler-delay domain. Performance is compared for uncoded OTFS and OFDM transmissions using a Jakes's channel model, with OTFS significantly outperforming OFDM in terms of bit error rate (BER) due to the channel hardening effect provided by the OTFS pre- and post-processing. It is noted in [4] that with OTFS applied as a processing block either side of OFDM, it is not a capacity enhancing technique

per-se. In [5] the authors suggest that any orthogonal spreading sequence applied across time and frequency can capture the same diversity as OTFS. This claim is supported with BER simulations. However, unlike general precodings, OTFS benefits from having a sparse channel response where every symbol experiences the same gain (for ideal pulses); properties that can be exploited in equalisation and channel estimation.

Many of the existing works assume the use of 'ideal' pulse-shaping wherein there is no interference across time or frequency. According to the uncertainty principle, these ideal pulses are unrealisable [3]. In [3] the use of realistic rectangular pulses without the use of a cyclic prefix is analysed and it is found through simulations, that these give the same performance as ideal pulses but with a more complex channel response.

A. Contributions

The main contributions of this paper are as follows:

- We analyse the use of practical rectangular transmit and receive pulses with cyclic prefix, deriving a simple modified expression for the Doppler-delay channel output in terms of the delays and Doppler shifts of the paths.
- We compare the performance of coded OTFS and OFDM in realistic environments at both sub-6 GHz and mmWave frequencies, using channels obtained using ray launching. The ray launching simulations include the effects of diffuse scattering, an important propagation mechanism at mmWave and accurately calculate Doppler shifts accounting for motion within the channel.

III. SYSTEM MODEL

Following the outline in [1], NM QAM symbols, $x[k,l]$, are arranged on a $N \times M$ grid in the Doppler-delay domain. These are mapped to an $N \times M$ grid, $X[n,m]$ in the time-frequency domain using the inverse symplectic Fourier transform,

$$X[n,m] = \frac{1}{\sqrt{NM}} \sum_{k=0}^{N-1} \sum_{l=0}^{M-1} x[k,l] e^{j2\pi(\frac{nk}{N} - \frac{ml}{M})}. \quad (1)$$

A time-frequency modulator or Heisenberg transform is then used to produce the time domain signal, $s(t)$, using transmit pulse $g_{tx}(t)$.

$$s(t) =$$
$$\frac{1}{\sqrt{NM}} \sum_{n=0}^{N-1} \sum_{m=0}^{M-1} X[n,m] g_{tx}(t-nT_s) e^{j2\pi m\Delta f(t-nT_s)}$$
$$(2)$$

where T_s represents the OFDM symbol spacing and Δf the OFDM subcarrier spacing. The signal is passed through a doubly dispersive channel characterised by

impulse response $h(\tau,\nu)$ with delay Doppler parameters τ and ν, to give received signal $r(t)$,

$$r(t) = \int\int h(\tau,\nu) s(t-\tau) e^{j2\pi\nu(t-\tau)} d\tau d\nu. \quad (3)$$

The receiver performs matched filtering with receive pulse $g_{rx}(t)$ to compute the cross ambiguity function $A_{g_{tx},r}(t,f)$.

$$Y(t,f) = A_{g_{tx},r}(t,f) =$$
$$\int g_{rx}^*(t'-t) r(t') e^{-j2\pi f(t'-t)} dt'. \quad (4)$$

This is sampled at $t = nT_s, f = m\Delta f$ to give the matched filter output on an $N \times M$ time-frequency grid as

$$Y[n,m] = A_{g_{tx},r}(nT_s, m\Delta f). \quad (5)$$

A receive window function, $W[n,m]$, is then applied before the Doppler-delay symbols are recovered using the symplectic Fourier transform

$$y[k,l] =$$
$$\frac{1}{\sqrt{NM}} \sum_{n=0}^{N-1} \sum_{m=0}^{M-1} W[n,m] Y[n,m] e^{-j2\pi(\frac{nk}{N} - \frac{ml}{M})}. \quad (6)$$

A ray-based quasi-static propagation channel is assumed, consisting of L paths between transmitter and receiver, each with gains h_i, delays τ_i and Doppler shifts ν_i, giving an impulse response

$$h(\tau,\nu) = \sum_{i=1}^{L} h_i \delta(\tau-\tau_i) \delta(\nu-\nu_i). \quad (7)$$

IV. INPUT-OUTPUT RELATIONSHIP OF OTFS

A. Ideal Pulses

For ideal transmit and receive pulses obeying the 'bi-orthogonality condition', the effect of the doubly dispersive channel is a simple multiplication in the time-frequency domain,

$$Y[n,m] = H[n,m] X[n,m]. \quad (8)$$

The dual of this in the Doppler-delay domain is a circular convolution of the QAM symbols with the windowed, periodic, channel impulse response given by

$$y[k,l] = \sum_{m=0}^{M-1} \sum_{n=0}^{N-1} x[n,m] h_w[k-n, l-m] \quad (9)$$

where

$$h_w[k,l] =$$
$$\frac{1}{NM} \sum_{n=0}^{N-1} \sum_{m=0}^{M-1} W[n,m] H[n,m] e^{-j2\pi(\frac{nk}{N} - \frac{ml}{M})}. \quad (10)$$
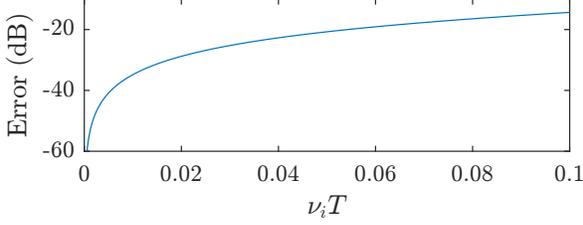
Fig. 1. Error of the approximate channel expression defined in (15).

B. Rectangular Pulse with Cyclic Prefix

As ideal pulses that perfectly fulfil the bi-orthogonality condition cannot be realised, practical rectangular transmit and receive pulses are instead considered. Specifically, we consider a system employing standard OFDM modulation with a cyclic prefix, characterised by

$$
g_{tx}(t) = \begin{cases} \frac{1}{\sqrt{T}}, & -T_{cp} \le t \le T. \\ 0, & \text{otherwise.} \end{cases} \tag{11}
$$

$$
g_{rx}(t) = \begin{cases} \frac{1}{\sqrt{T}}, & 0 \le t \le T. \\ 0, & \text{otherwise.} \end{cases} \tag{12}
$$

where T_{cp} is the cyclic prefix length, $T = 1/\Delta f$, and $T_s = T + T_{cp}$.

1) Time-Frequency Domain: Following a similar derivation to [4], it can be shown that for general rectangular pulses the channel operation is given by

$$
Y[n,m] = \sum_{m'=0}^{M-1} H_m[n,m']X[n,m'], \tag{13}
$$

where the summation over m' represents inter-carrier interference, according to

$$
H_m[n,m'] =
$$
$$
\sum_{i=1}^{L} h_i \frac{1-e^{j2\pi\nu_i T}}{j2\pi(m-m'-\nu_i T)} e^{-j2\pi(m\Delta f\tau_i - \nu_i nT_s)}. \tag{14}
$$

However, for sufficiently large sub-carrier spacing ($\nu_i T \ll 1$), the inter-carrier interference becomes negligible and the desired gain is well approximated by a first order Taylor series expansion at $\nu_i T = 0$.

$$
\frac{1-e^{j2\pi\nu_i T}}{j2\pi(m-m'-\nu_i T)} \approx \begin{cases} 1 + j\pi\nu_i T, & m' = m \\ 0, & \text{otherwise.} \end{cases} \tag{15}
$$

The error of this approximation is shown in Fig. 1. Therefore, for small values of $\nu_i T$ the multiplicative channel model of (8) and (9) is a good approximation, with

$$
H[n,m] = \sum_{i=1}^{L} h_i' e^{-j2\pi(m\Delta f\tau_i - \nu_i nT_s)}. \tag{16}
$$

$$
h_i' = h_i(1 + j\pi\nu_i T) \tag{17}
$$

2) Doppler-delay domain: For small $\nu_i T$, the channel performs a circular convolution between the windowed impulse response in (10) and the QAM symbols. Applying a rectangular window, $W[n,m] = 1$, the channel impulse response is

$$
h[k,l] = \sum_{i=1}^{L} h_i' F(\nu_i T_s - k) G(\tau_i \Delta f - l). \tag{18}
$$

This impulse response is the sum of L different pulses, shifted by (ν_i, τ_i) and then spread according to the functions

$$
F(\nu_i T_s - k) = \frac{1}{N} \left(\frac{1 - e^{j2\pi(\nu_i NT_s - k)}}{1 - e^{j2\pi(\nu_i T_s - k/N)}} \right) \tag{19}
$$

$$
G(\tau_i \Delta f - l) = \frac{1}{M} \left(\frac{1 - e^{-j2\pi(M\Delta f\tau_i - l)}}{1 - e^{-j2\pi(\Delta f\tau_i - l/M)}} \right). \tag{20}
$$

This 'smearing' results from the implicit windowing that occurs when sampling the time-frequency domain over a finite region, defined by the total bandwidth $B = M\Delta f$ and symbol duration $T_d = NT_s$. The resolution to which the multipath components can be resolved in the delay and Doppler dimensions is $\Delta\tau = \frac{1}{B}$ and $\Delta\nu = \frac{1}{T_d}$.

V. CHANNEL CODING & EQUALISATION

In our simulations we compare the performance of OTFS to OFDM. For a meaningful comparison, we employed channel coding, namely 3/4 rate LDPC codes with a block length of 672 bits. Each OTFS symbol or set of N OFDM symbols consisted of multiple coded blocks, with the coded bits randomly mapped to the NM QAM symbols. The NM QAM symbols are then mapped to the $N \times M$ grid in the Doppler-delay or time-frequency domains for OTFS and OFDM respectively. An iterative message passing decoder was employed at the receiver.

To recover the QAM symbols, equalisation was performed at the receiver in both the time-frequency domain (OTFS/OFDM) and Doppler-delay domain (OTFS). We assumed that the receiver had full knowledge of the channel as defined in (16), but did not cancel the inter-carrier interference resulting from the use of non-ideal pulses. It should be noted that OTFS has some benefits when obtaining this channel knowledge, as it can be captured using a single transmitted pilot symbol, as discussed in [6].

A. Time-Frequency Equalisation

In the time-frequency domain, a linear minimum mean square error windowing function was employed for both OFDM and OTFS, defined as

$$
W[n,m] = \frac{H[n,m]^*}{|H[n,m]|^2 + N_0} \tag{21}
$$

Where N_0 is the receiver noise power. With OFDM, soft symbol estimates (bit log-likelihood ratios, LLRs) were

then passed to the decoder. For OTFS, the window partially cancels interference, and ensures a sparse Doppler-delay impulse response, $h_w[k, l]$, with most values close to zero. A second equalisation stage was then employed in the Doppler-delay domain.

B. Doppler-Delay Equalisation

In order to better capture the channel diversity for OTFS, the windowing is followed by a low complexity message passing equaliser based on the message passing with Gaussian interference approximation algorithm outlined in [7], and also applied in [3]. The circular convolution in (10) can be rewritten in matrix form as

$$\mathbf{y} = \mathbf{H}_w \mathbf{x} \approx \bar{\mathbf{H}}_w \mathbf{x}, \tag{22}$$

where $\bar{\mathbf{H}}_w$ is a sparse approximation of $\mathbf{H}_w$ given by

$$\left(\bar{\mathbf{H}}_w\right)_{i,j} = \begin{cases} \left(\mathbf{H}_w\right)_{i,j}, & \left|\left(\mathbf{H}_w\right)_{i,j}\right| > \alpha \\ 0, & \text{otherwise,} \end{cases} \tag{23}$$

for appropriately chosen α. The message passing equaliser exploits the sparsity of $\bar{\mathbf{H}}_w$ to iteratively estimate the posterior symbol probabilities and then output the corresponding LLRs to the decoder.

VI. RAY LAUNCHING SIMULATIONS

Ray launching was used to simulate the propagation channel between a mobile station and a base-station at 3.5 GHz and 28 GHz, designated frequency bands for future 5G systems. This propagation modelling technique captures the spatial characteristics of the channel and allows the parameters h_i, τ_i and ν_i to be explicitly calculated for given transmitter (TX) and receiver (RX) locations within a 3D model of an environment.

The ray launching tool is an in house model. Rays are fired "equally" from a source in three dimensions. Ten thousand rays were used, corresponding to an angular resolution of 0.035 rads. The ray launcher is, at the time of writing, not fully verified against measurements. Below, we provide details on the propagation models and parameters used in the ray launching simulations.

A. Power of Individual Paths

In general, each ray path between TX and RX consists of one or more ray segments. The received power of the ith ray path, $|h_i|^2$, is calculated by multiplying linear power gains and losses along that path. This includes antenna gains at the TX/RX $\mathbf{G}_{TXi/RXi}$, losses due to reflection/scattering for the jth interaction, $\mathbf{K}_{[i,j]}$, and losses due to propagation in free space, P_i. Apart from P_i, these are 2×2 matrices specifying co- and cross-polar coefficients for vertical and horizontal polarisation. For the simulations in this paper, the transmitted power is vertically polarised and only the vertical channel is observed at the RX. Rotation matrices, $\mathbf{R}[i, j]$, were used to resolve a polarisation vector into a local vertical

and horizontal polarisation before interaction with a primitive, as in [8]. The total loss for a given ray path is given by (24) where $\mathbf{b} = \begin{bmatrix} 1 & 0 \end{bmatrix}^T$.

$$|h_i|^2 = \mathbf{b}^T \mathbf{G}_{TXi} \mathbf{R}_{[i,0]} \mathbf{K}_{[i,0]}..\mathbf{K}_{[i,m]} \mathbf{R}_{[i,m+1]} \mathbf{G}_{RXi} \mathbf{b} P_i \tag{24}$$

where the propagation path loss is calculated according to (25) with d as the distance for the ray path in meters and λ is the wavelength in meters. To limit L in simulations and therefore keep computation tractable, rays below a power threshold were destroyed.

$$P_i = \left(\frac{\lambda}{4\pi d}\right)^2 \tag{25}$$

In the case that the jth interaction is a specular reflection, $\mathbf{K}_{[i,j]}$ corresponds to the Fresnel reflection matrix, reduced by a factor to account for the roughness of the surface [9]. This reduction factor is shown in (26) below.

$$\kappa(\sigma) = \exp\left[-\left(\frac{4\pi\sigma\cos(\theta)}{\lambda}\right)^2\right] \tag{26}$$

where λ is the wavelength in meters, θ is the angle of incidence, and σ is the standard deviation of the height of the surface in meters.

The phase of each h_i is the cumulative phase shift from the reflections along that path,

$$\angle h_i = \phi_{TXi} + \phi_{i,0} + \ldots + \phi_{i,m} + \phi_{RXi}. \tag{27}$$

B. Scattering

At 28 GHz diffuse scattering is an important propagation mechanism. To simulate this mechanism, a version of the Kirchhoff model [10]-[11], which was verified in [12], was used in the ray launching tool. The ray model simulated up to five reflections and one diffuse scatter, considering diffuse scatters only for either the last interaction before arriving at the RX, or the first interaction after leaving the TX. In the case $\mathbf{K}_{[i,j]}$ was the matrix for a diffuse scatter it was formulated as shown in [8]-[9],[13]. The area of a scattering tile is calculated based on the distance from the source and angle between rays.

C. Dynamic Scenarios Simulated

Two scenarios were simulated. The first was a section of motorway as shown in Fig. 2, with bridges, billboards and crash barriers included. The other scenario was a city, based on a small section of London, England, as shown in Fig. 3. The cars and billboards were made of metal and the road surface, bridges, buildings and crash barriers were concrete. Table I shows the parameters used for these materials including relative permittivity, ϵ, and correlation length, Ω, which is defined in [10][14]. For metallic surfaces diffuse scattering was not simulated due to their relative high smoothness.

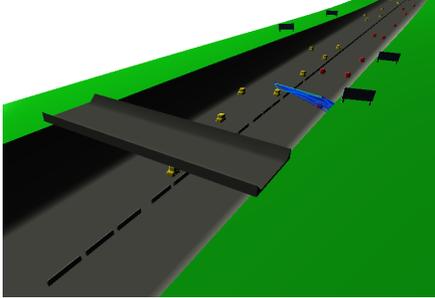| Material	ϵ	σ (m)	Ω (m)
Metal	9+3000j	0	0.1
Concrete	3+3j	4.1×10^{-4}	1.3×10^{-3}

TABLE I
PROPERTIES OF THE MATERIALS CONSIDERED IN SIMULATIONS.

Fig. 2. Motorway scenario.
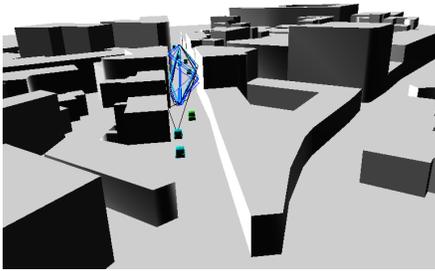
Fig. 3. Town scenario, contains information from open street maps, which is made available at https://www.openstreetmap.org under the Open Database License (ODbL) https://opendatacommons.org/licenses/odbl/.

In both cases a straight route of 40 m was traversed in 2 m steps by the TX, with the RX being a stationary base station. In the motorway the base-station antenna was at a height of 9 m and was 5 m across the road from the TX, which was at a 1.1 m height. The TX started 30 m away from the BS, moving past the base-station at a velocity of 112 km/h (31 m/s). In the town the base-station was at a 15m height, a height similar to the rooftops. The TX was at 1 m height and started at a position 15 m from the base-station moving along the street away from it at a velocity of 48 km/h (13 m/s). The locations of the cars were updated based on their velocity at each time-step in order to properly represent the dynamic scene. At all simulated locations, a clear line-of-sight path between TX and RX existed.

D. Doppler Shifts

In existing work it is assumed that many propagation paths will exist, with uniformly distributed angle of arrival and thus random Doppler shifts. This is unrealistic for real line-of-sight channels. In Fig. 4 the Doppler power spectrum for the channel at 28 GHz on the motorway is shown for each position on the route. This

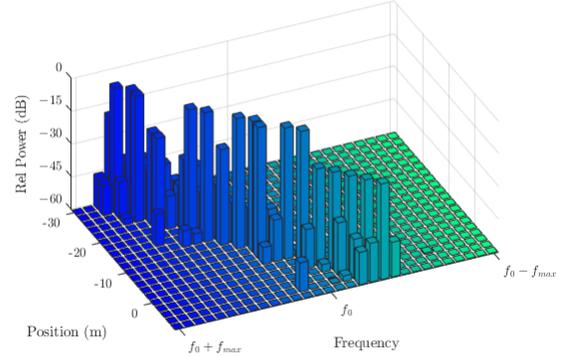should be contrasted to the classic "bathtub" Doppler power spectrum of Jakes's model.

Fig. 4. Doppler power spectrum along the route at 28 GHz.

We calculated the Doppler shift, ν_i, for each of the i ray paths between the TX and the RX. For each ray segment the apparent frequency at the end of the ray segment was calculated using,

$$f_{n+1} = \left(\frac{c + \boldsymbol{u}_r \cdot \hat{\boldsymbol{d}}_n}{c + \boldsymbol{u}_s \cdot \hat{\boldsymbol{d}}_n} \right) f_n \qquad (28)$$

where f_n is the frequency at the start of the ray segment, $\boldsymbol{u}_r$ and $\boldsymbol{u}_s$ are receptor and source velocity vectors respectively, $\hat{\boldsymbol{d}}_n$ is a unit direction vector describing the direction of propagation along the nth ray segment, c is the speed of the wave in the medium and f_{n+1} is the apparent frequency at the receptor due to the Doppler shift.

With f_0 equal to the carrier frequency, (28) was used in conjunction with (29) to calculate ν_i, the Doppler shift on the ith ray path, where the ith path had m ray segments, as

$$\nu_i = f_m - f_0. \qquad (29)$$

E. Antenna Patterns

Directional antennas are generally used in millimetre wavelength communication systems to mitigate interference, overcome propagation losses and blockage caused by moving objects [15]. The antennas have the effect of spatially filtering the channel. A simple directional "pattern" with a beam-width of $15°$ was applied according to (30), to point directly "along" the strongest propagation path for channels captured at 28 GHz.

$$G_i = \begin{cases} 31.6, & \theta_i \leq 7.5° \\ 0.87, & \text{otherwise.} \end{cases} \qquad (30)$$

In (30), G_i is the linear antenna directivity for the ith ray and θ_i is the angle between the ith ray and the strongest omnidirectional ray. These linear directivities
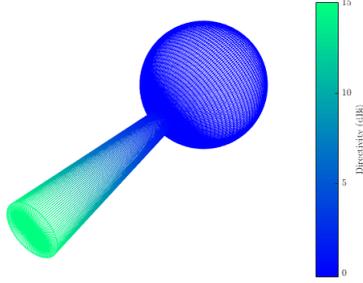
Fig. 5. Antenna "pattern" used for 28 GHz channels.

f_0	Δf	M	N
28 GHz	60 kHz	1667	7
3.5 GHz	30 kHz	667	14

TABLE II
SIMULATION CONFIGURATIONS.

correspond to 15 dB and -0.6 dB. The gains prescribed by (30) were applied separately at both the TX and the RX for each ray path. This pattern is shown in Fig. 5.

Whilst the moving TX antenna was floating in free space in simulations, it was supposed to represent a roof mounted antenna on a car so any path within 80° of the direction directly down was removed to account for attenuation by the shadowing of the car.

VII. SIMULATION RESULTS AND ANALYSIS

Bit level simulations were carried out at both frequencies for each of the environments using the system parameters in Table II. These parameters were chosen to fit loosely with the 5G-NR physical layer specification, with the length of the OTFS symbols chosen to fit within one transmission frame. Subcarrier spacing was chosen to keep intercarrier interference to a minimum in accordance with Fig. 1. Total transmission bandwidths of 100MHz and 20MHz were used at 28 GHz and 3.5 GHz respectively. To remove the effects of slow fading, transmit power was chosen such that the received signal to noise ratio (SNR) was the same at each position along the route. A carrier offset was applied at the TX such that at the RX the Doppler shift of the strongest path was equal to zero.

Fig. 6 shows the block error rate for the motorway environment as the TX moves along the route. It can be seen that OTFS outperforms OFDM at both 3.5 GHz and 28 GHz, with a fairly constant performance gap between the two. We note that despite the constant SNR along the route, the performance of both OFDM and OTFS varies considerably, especially at 3.5 GHz. Inspection of the channels at the positions at which a high block error rate was observed found that at these locations there were multiple significant paths between TX and RX, causing deep fades in the time-frequency domain, or higher interference in the Doppler-delay domain, and
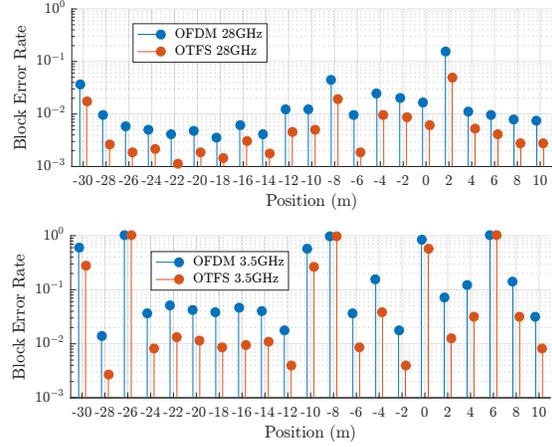

Fig. 6. Block error rate for motorway environment, 31m/s, at 28 GHz (top) and 3.5 GHz (bottom), with 16QAM, 3/4 Rate, 11.5 dB SNR

therefore reducing performance. The lower variation in error in the mmWave channel we attribute to the relative sparsity of channel, which was dominated by the line-of-sight path, due to the increased path loss of reflected paths that occurs at these frequencies and spatial filtering by the directive antenna (see Fig. 4).
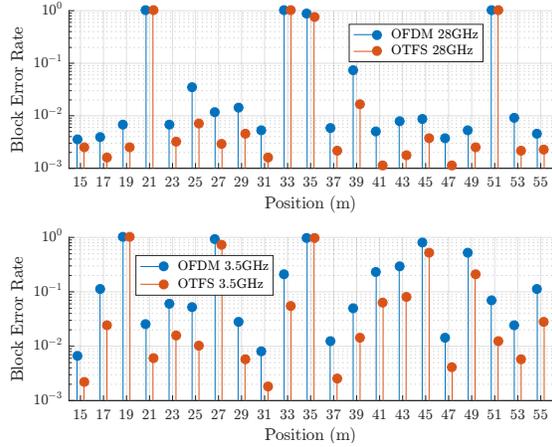

Fig. 7. Block error rate for town environment, 13m/s, at 28 GHz (top) and 3.5 GHz (bottom), with 16QAM, 3/4 Rate, 11.5 dB SNR.

Fig. 7 shows the block error rate for the town environment. OTFS again outperforms OFDM at all positions along the route, at both frequencies. Whilst with the TX and vehicles moving at lower speed, the maximum Doppler shift is lower for this environment, the built up environment provides a richer scattering environment, causing more fading/interference at both 3.5 GHz and 28 GHz.

These initial results indicate that OTFS can offer performance benefits over OFDM in automotive mobility scenarios, and that further investigation is due. Topics for future work include a performance comparison of the two waveforms using longer block codes and more

detailed study of link level performance with channel estimation.

VIII. CONCLUSION

In this paper we have compared the performance of OTFS and OFDM in realistic vehicle to infrastructure 3D modelled environments, using ray-launching simulations to calculate the power, delay and Doppler shifts of propagation channels at sub-6 GHz and mmWave frequencies. Using practical rectangular pulse shapes and short LDPC block codes, it was found that OTFS outperforms OFDM in terms of block error rate by more than 50% in a low mobility built-up urban environment, and high mobility motorway environment, at both 3.5 GHz and 28 GHz.

ACKNOWLEDGEMENT

REFERENCES

[1] R. Hadani, S. Rakib, M. Tsatsanis, A. Monk, A. J. Goldsmith, A. F. Molisch, and R. Calderbank, "Orthogonal Time Frequency Space Modulation," in *2017 IEEE Wireless Communications and Networking Conference (WCNC)*, pp. 1–6, March 2017.

[2] R. Hadani, S. Rakib, A. F. Molisch, C. Ibars, A. Monk, M. Tsatsanis, J. Delfeld, A. Goldsmith, and R. Calderbank, "Orthogonal Time Frequency Space (OTFS) modulation for millimeter-wave communications systems," in *2017 IEEE MTT-S International Microwave Symposium (IMS)*, pp. 681–683, June 2017.

[3] P. Raviteja, K. T. Phan, Y. Hong, and E. Viterbo, "Interference cancellation and iterative detection for Orthogonal Time Frequency Space modulation," *ArXiv e-prints*, Feb. 2018.

[11] A. Torabi and S. A. Zekavat, "Directional channel modelling for millimetre wave communications in urban areas," *IET Communications*, vol. 12, no. 6, pp. 656–664, 2018.

[4] A. RezazadehReyhani, A. Farhang, M. Ji, R. R. Chen, and B. Farhang-Boroujeny, "Analysis of discrete-time MIMO OFDM-based Orthogonal Time Frequency Space modulation," *ArXiv e-prints*, Oct. 2017.

[5] T. Zemen, M. Hofer, D. Loeschenbrand, and C. Pacher, "Iterative detection for orthogonal precoding in doubly selective channels," *ArXiv e-prints*, Oct. 2017.

[6] M. Kollengode Ramachandran and A. Chockalingam, "MIMO-OTFS in high-doppler fading channels: signal detection and channel estimation," *ArXiv e-prints*, May 2018.

[7] T. L. Narasimhan and A. Chockalingam, "Detection and decoding in large-scale MIMO systems: A non-binary belief propagation approach," in *2014 IEEE 79th Vehicular Technology Conference (VTC Spring)*, pp. 1–5, May 2014.

[8] S. Priebe, M. Jacob, and T. Krner, "Polarization investigation of rough surface scattering for THz propagation modeling," in *Proceedings of the 5th European Conference on Antennas and Propagation (EUCAP)*, pp. 24–28, April 2011.

[9] B. Petr and S. Andre, *The scattering of electromagnetic waves from rough surfaces.* The Artech House radar library, Norwood, MA: Artech House, 1963.

[10] C. Jansen, S. Priebe, C. Moller, M. Jacob, H. Dierke, M. Koch, and T. Kurner, "Diffuse scattering from rough surfaces in THz communication channels," *IEEE Transactions on Terahertz Science and Technology*, vol. 1, pp. 462–472, Nov 2011.

[12] S. A. M. Tariq, C. Despins, S. Affes, and C. Nerguizian, "Rough surface scattering analysis at 60 GHz in an underground mine gallery," in *2014 IEEE International Conference on Communications Workshops (ICC)*, pp. 724–729, June 2014.

[13] S. Priebe, M. Jacob, C. Jansen, and T. Krner, "Non-specular scattering modeling for THz propagation simulations," in *Proceedings of the 5th European Conference on Antennas and Propagation (EUCAP)*, pp. 1–5, April 2011.

[14] L. Sayer, A. Loaiza Freire, E. Mellios, and A. Nix, "A Kirchhoff scattering model for millimetre wavelength wireless links," in *2018 12th European Conference on Antennas and Propagation (EUCAP 2018)*, 2018.

[15] T. S. Rappaport, Y. Xing, G. R. MacCartney, A. F. Molisch, E. Mellios, and J. Zhang, "Overview of millimeter wave communications for fifth-generation (5G) wireless networks x2014;with a focus on propagation models," *IEEE Transactions on Antennas and Propagation*, vol. 65, pp. 6213–6230, Dec 2017.